Chapter 5

Custom EIT Meshes

This work has been presented in part at: the 21st International Conference on Biomedical Applications of Electrical Impedance Tomography (EIT 2021) (Stowe et al.*, 2021b).*

Acknowledgement

Tidal Medical funded the work presented in this chapter.

5.1 Introduction

Acute respiratory distress syndrome ARDS is a form of respiratory failure caused by widespread swelling and accompanied by an accumulation of fluid in the lungs. ARDS is a challenging disease to diagnose and treat. No gold standard test exists for diagnosis, and few treatments are effective (Pham and Rubenfeld, 2017).

The mortality rate is estimated to be as high as 40% (Abe *et al.*, 2018). Early studies on the pathology of ARDS identified the effectiveness of adjusting positive end-expiratory pressure PEEP to improve oxygenation in patients (Ashbaugh *et al.*, 1967; Petty, 2001), and recent research suggests that treatment strategies to reduce lung injury during ventilation outperform pharmacological interventions (Duggal *et al.*, 2015). Monitoring ARDS patients during ventilation is vital to ensure that ventilator-induced lung injury is avoided (Bates and Smith, 2018), but few appropriate techniques are available. Computed tomography (CT) images used for diagnosis are inappropriate for continuous use due to ionizing radiation exposure, and other global parameters of lung function may not give an accurate estimate of lung homogeneity (Zhao *et al.*, 2009).

Electrical impedance tomography EIT was proposed as a monitoring technique for ARDS patients since it is non-invasive and can safely monitor and image the lungs in real time (Denaï *et al.*, 2010; Frerichs *et al.*, 2017). One of the most useful parameters to classify lung ventilation with EIT has been global inhomogeneity GI (Hochhausen *et al.*, 2019; Hough *et al.*, 2016; Hsu *et al.*, 2017; Humphreys *et al.*, 2011; Šribar *et al.*, 2020; Zhao *et al.*, 2012). GI has been identified as a clinically useful parameter to monitor ventilation (Frerichs and Becher, 2019).

The largest issue with using EIT for regional ventilation monitoring is that incorrectly modelling the boundary can introduce a large artefact in reconstructed images (Grychtol *et al.*, 2012). The correct lung boundary is also required to calculate the GI metric (Zhao *et al.*, 2009). Incorrectly modelling the boundary and lung area when investigating regional homogeneity can lead to an incorrect GI es-

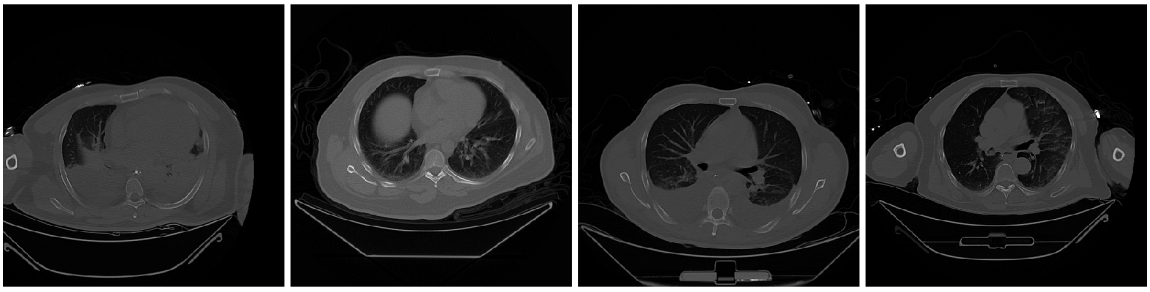

Figure 5.1: Raw CT data from 4 subjects taken at the 4^{th} intercostal space. This image highlights the challenges with automatic segmentation of the lung and external boundary. In some subjects the external boundary is obscured by the arms, and in other subjects the true lung boundary is masked by occlusions.

timate (Yang *et al.*, 2021). Yang *et al.* (2021) found that a model with custom segmented external and lung boundaries was more sensitivite to changes in lung condition using GI compared with generic models. This suggests a custom mesh with more defined lung regions may also improve sensitivity to lung-based pulsatility and improve measures of perfusion.

Custom meshes have been created by segmenting the boundaries of lungs and organs to monitor ARDS (Yang *et al.*, 2021), but automatic segmentation of the lung region for a range of ARDS patients is a challenging problem. Typically ARDS patients will have a combination of swelling, fluid and lung collapse obscuring the true boundary of the lungs. Figure 5.1 depicts unprocessed CT slices of the 4^{th} intercostal space from 4 subjects with ARDS. This figure highlights the challenges of automatically segmenting lung tissue across several subjects. In some CT images, the arms obscure the external boundary, and in other CT images partial or total occlusions mask the true lung boundary.

This chapter introduces a tool that enables quick segmentation of the lungs and exterior boundary to facilitate individualized bedside monitoring and guide treatment

of ARDS. This tool processes and automatically segments the external and lung boundaries in diagnostic CT images, then presents them for manual correction to create custom EIT models. The goal of this chapter is to generate custom models that improve sensitivity in the lung regions and produce custom, accurate meshes to facilitate real time, individualized ventilation monitoring for ARDS patients.

5.2 Methods

This section presents the methodolgy for:

- Automatic segmentation of diagnostic CT images (section 5.2.1)
- Design of a manual segmentation correction tool (section 5.2.2)
- Mesh generation (section 5.2.3)
- Comparison of GI index between generic and custom EIT models (section 5.2.4)

Figure 5.2 shows a summary of the mesh generation process from raw diagnostic CT data to a custom mesh based on the geometry of the patient.

For image segmentation and the manual correction interface Matlab 2021a (Mathworks, USA) with the image processing toolbox was used. Mesh generation and reconstruction was performed with EIDORS 3.10 (Adler *et al.*, 2017a) using Matlab 2019b. At the time of writing Matlab 2019b was required to use some EIDORS functionality, but Matlab 2021a provided some additional features that improved responsiveness of the graphical user interface GUI.

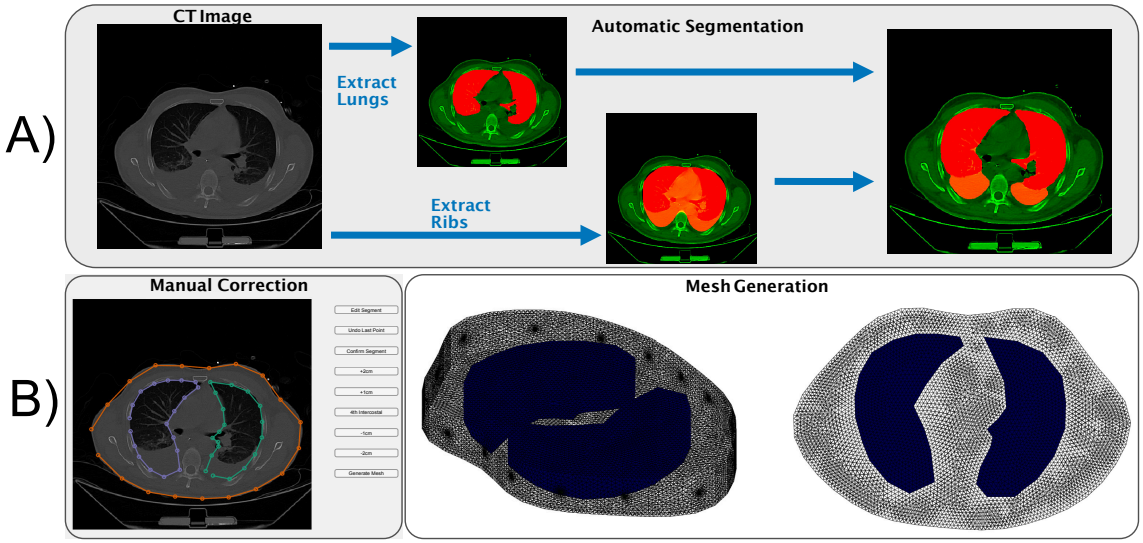

Figure 5.2: An overview of the segmentation and editing process showing: A) A sample raw CT which was thresholded, scaled and adjusted over several adjacent slices to identify the lung regions and an enclosed rib area, and the resulting lung estimate; and B) A screen capture of the manual mesh correction process and 2 views of the generated mesh.

5.2.1 Automatic segmentation of the thorax

Automatic segmentation of lung regions in ARDS patients is challenging due to the variability in lung tissue intensity, and the presence of fluid or collapsed lung regions. In some patients the lung regions were not visible in the image and even manual correction of the segmentation required estimation. This automatic technique identifies the chest cavity using several adjacent slices to locate the ribs. Even when no lung is visible in the image, this produces a starting point close to the expected boundary to reduce correction time. This tool is designed to segment the true lung boundary as closely as possible to simplify manual correction. If no ribs or lung are detected, ellipses are placed within the boundary close to the expected lung location that can be corrected manually.

The automatic segmentation uses a diagnostic CT image with the slice corresponding to the 4^{th} intercostal space identified. To begin segmentation, the user must select the series of CT images they wish to segment, and the frame number that corresponds to the 4th intercostal space. For the 4 test subjects, the 4^{th} intercostal space was identified manually using 3D Slicer 4 (Fedorov *et al.*, 2012), as the space between the 4^{th} and 5^{th} ribs underneath the arm. This location corresponded to the electrode belt placement for EIT measurements.

A detailed algorithmic outline of the automatic segmentation process is presented in appendix A.

5.2.1.1 External boundary

The boundary segmentation steps are shown in figure 5.3. To segment the boundary, the selected raw CT slice (A in figure 5.3) was adjusted so that the intensity of the lung tissue was 0 and the maximum image value was 1 (B in figure 5.3). Next the image was eroded and reconstructed to remove small features and retain large structures (C in figure 5.3). Finally, the image was binarized (D in figure 5.3), and holes were filled (E in figure 5.3), to give the final boundary (F in figure 5.3).

5.2.1.2 Chest cavity

To segment the chest cavity 7 slices above and below the 4^{th} intercostal space were used giving 15 slices to segment. To begin, the external boundary of the selected slice was used (segmented using the method in section 5.2.1.1). The initial boundary (A in figure 5.4) was eroded to form a mask from the shrunken boundary shape (B

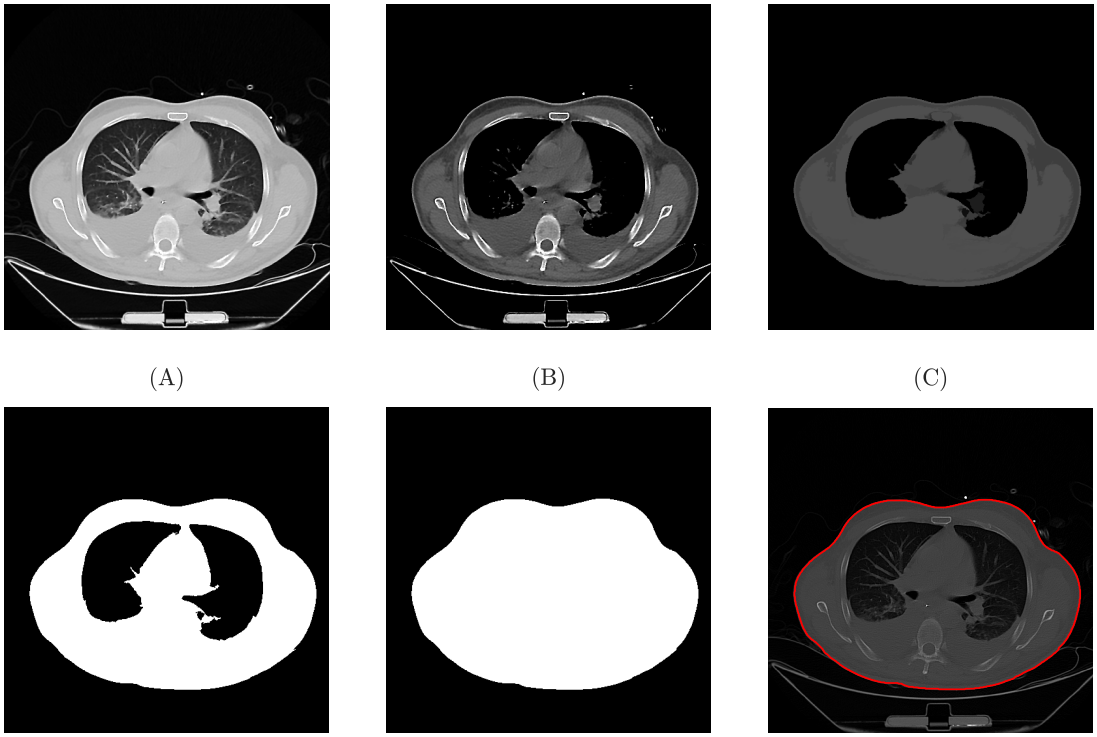

(A) (B) (C)

(D) (E) (F)

Figure 5.3: A raw CT image of the 4th intercostal slice (A) was adjusted based on the lung density (B), eroded and reconstructed (C), then binarized (D) and filled to give the final boundary (F).

in figure 5.4). This mask was used on a binarized image to extract bones and bright objects from within the thorax (C in figure 5.4). The image was closed to fill holes and identify bones (D in figure 5.4). Next all 15 adjacent slices were superimposed to combine all rib locations that occurred in more than one slice (E in figure 5.4). To fill holes in the ribcage, a rectangular element with a height of 5 and width of 50 was used to close the top half of the image (F in figure 5.4). A final thickening operation was performed to ensure continuity (G in figure 5.4). All objects connected to the boundary were removed to give the final chest cavity segmentation (H in figure 5.4).

5.2.1.3 Lungs

The lung segmentation was required to work in patients with ARDS and give an approximate lung boundary when the lungs were potentially collapsed or filled with fluid. To achieve this, a rough lung estimate based on the chest cavity was used together with a segmentation of the ventilated lung. The ventilated and non-ventilated regions of the lung were segmented based on the chest cavity segmentation (A in figure 5.5). First an estimation of the lung region was made by placing an ellipse in the centre of the chest cavity segmentation at the thinnest central point (B in figure 5.5). Next a ventilated lung estimate (C in figure 5.5) was made by inverting the binarized image from the external boundary segmentation (D in figure 5.3). Finally, a complete lung segmentation was generated by removing any part of the simple lung estimate (B in figure 5.5) that was within 5 pixels of the ventilated lung region, and combining the two lung estimates with a closing operation. This was able to give a close estimate of the lung boundary even in cases where little or no lung tissue was

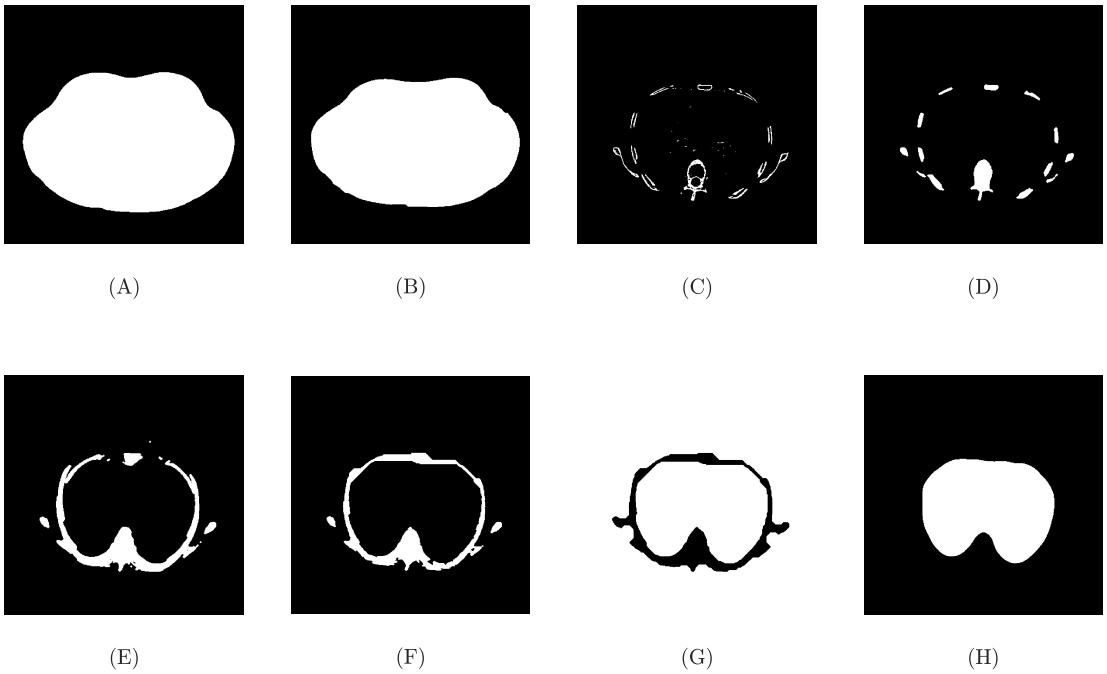

Figure 5.4: For each of the 15 selected slices the initial external boundary (A) was eroded to form a mask from the shrunken boundary shape (B). This mask was used on a binarized image to extract bones and bright objects from within the thorax (C). The image was closed to fill holes and identify bones (D). Next all 15 adjacent slices were superimposed to combine all rib locations that occurred in more than one slice (E). To fill holes, a rectangular element with a height of 5 and width of 50 was used to close the top half of the image (F). A final thickening operation was performed to ensure continuity (G). All objects connected to the boundary were removed to give the final chest cavity segmentation (H).

visually distinguishable.

5.2.2 Manual segmentation correction

Although the automatic segmentation was carefully designed to accurately segment the lungs, there were often cases where manual correction was required. To ensure accurate models were generated, an interface for manual correction was created. This tool allowed the user to correct the boundary for a selected CT slice. 20 points for each of the lungs and the external boundary were used for correction and placed over the corresponding CT image slice.

The segmentation correction tool was designed to save the segmentation with information on the selected image sequence and frame of the 4^{th} intercostal space for reference. The segmentation correction also allowed users to load and correct previously saved segmentations, or overwrite them completely. An example of the setup, and available input for the segmentation correction GUI is shown in figure 5.6. To make segmentation simpler, all data such as the frame of the 4^{th} intercostal space was saved after the initial data loading stage. Even if the segmentation was not completed, the user did not have to re-enter patient details when the CT was next loaded. An option was also added to manually input an adjustment value for the automatic segmentation of the ribs. If no ribs were detected during automatic segmentation, this could be used to adjust the threshold. This was not needed as the ribs were successfully identified in all test patients. The software was also designed to give informative error messages to enable troubleshooting, letting the user know if no ribs or no lungs were detected.

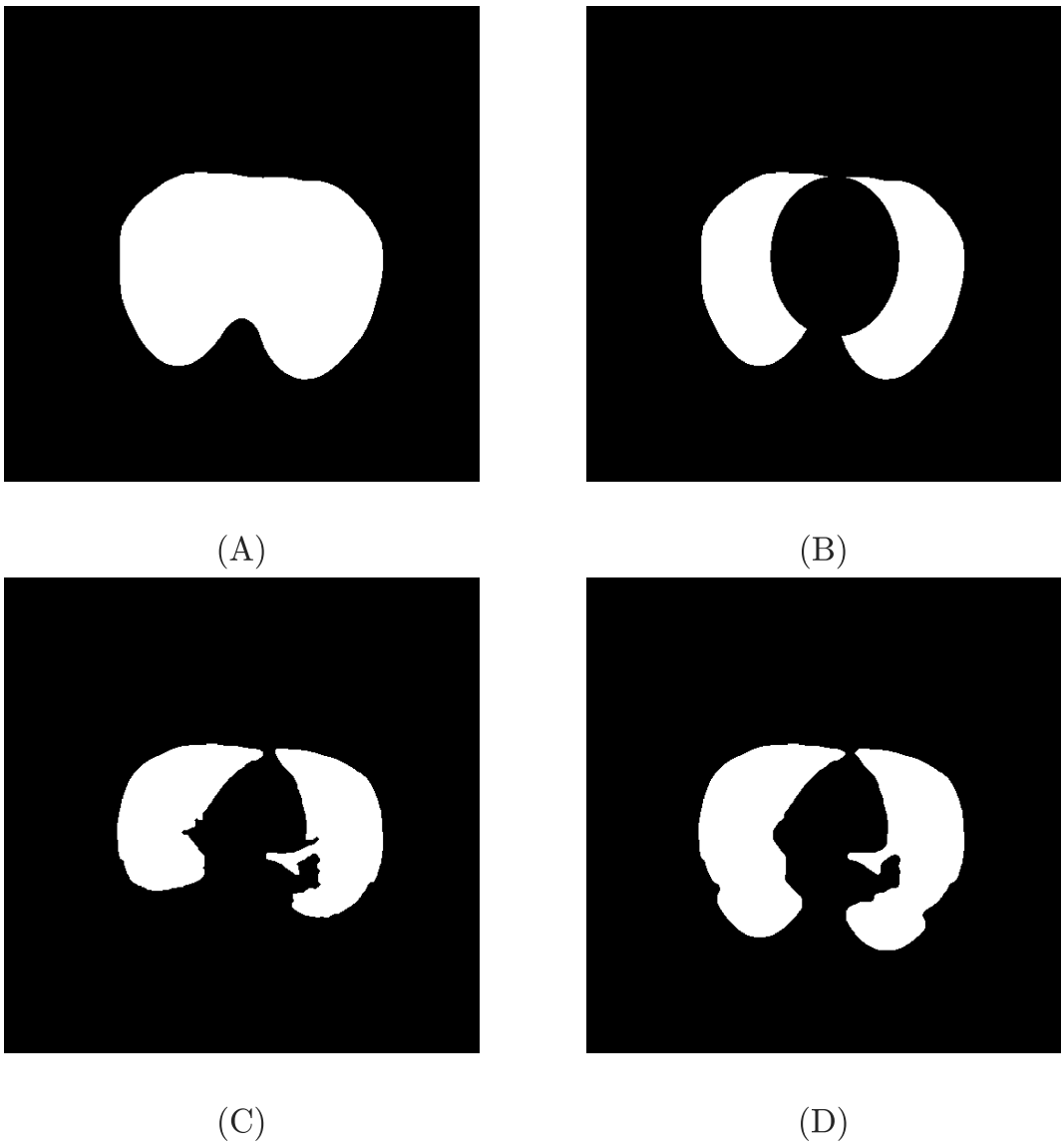

Figure 5.5: An approximation of the lung boundary was generated using the chest cavity segmentation (A) with an ellipse to remove the heart region (B). This was combined with a segmentation of the ventilated lung region (C) to give a total lung estimate (D).

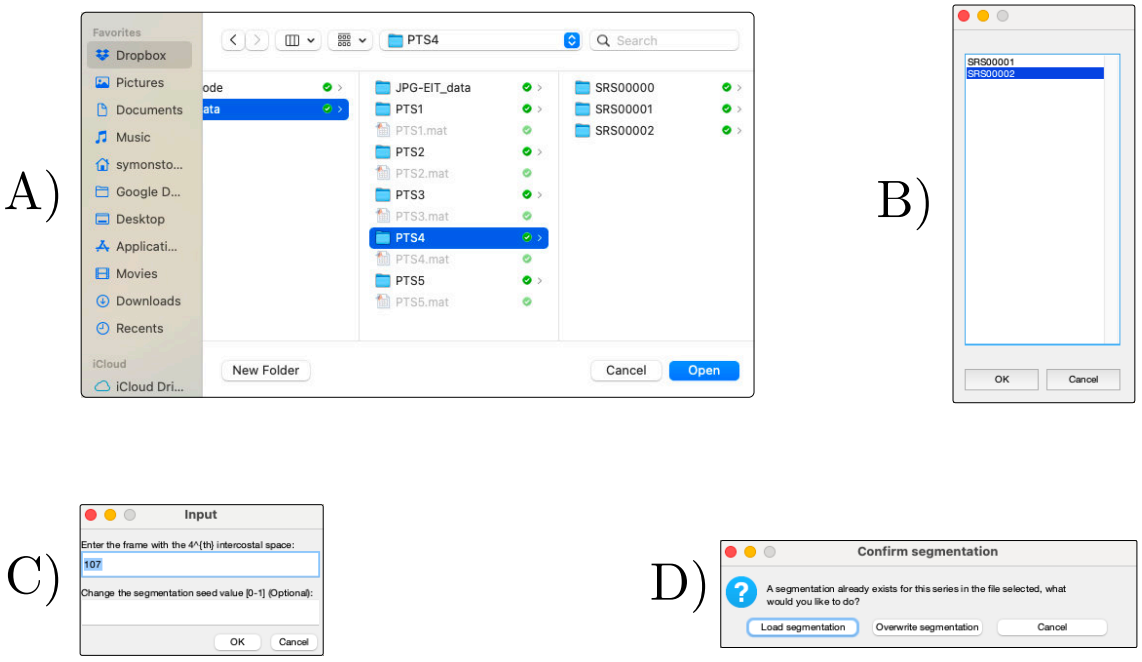

Figure 5.6: The data loading stages for the manual segmentation program are shown. A) A folder of patient data is selected. B) The desired CT data series is selected. C) The initial segmentation frame of the 4^{th} intercostal space is loaded from the patient settings file or input by the user. Optionally, an adjustment to the initial segmentation thresholding value can be input if the segmentation steps failed to locate ribs in the CT image. D) If an existing segmentation was saved, the user is asked before a new segmentation is made.

Figure 5.7: An example of a segmentation after being loaded into the segment editor program. The buttons on the right show the options available to the user, and the left shows the CT image for the corresponding slice with the automatic segmentation overlaid.

If an error was made during manual correction, the user could undo the last change or revert the selected point to the original location. Keyboard shortcuts were assigned to each of the functions to reduce the time required to segment each slice.

Figure 5.7 shows an example of the Matlab GUI for manually correcting the automatic segmentation. To segment, the user would click *Edit Segment* then select and move each point that required correction. The first click by the user selected the nearest point, and the subsequent click placed the point at the new location. Buttons on the side allowed the user to select the CT slice for correction, save the segmentation, and generate a mesh.

Figure 5.8: An example of a manually corrected segmentation with the arrow indicating the initial and new location of the last moved point. The selected point was moved for illustrative purposes and was not based on the initial segmentation.

After moving each point, an arrow was drawn between the original and new location of the point last moved to indicate the change and allow the user to see if the placement was correct. An example of a corrected slice showing the indicating arrow is shown in figure 5.8.

The end result was a GUI that allowed for quick correction of the automatic segmentation results. Spatial information from the DICOM image was also saved so that meshes could be designed to have the correct diameter and be correctly configured to the patient size.

5.2.3 Mesh generation

There is currently no available tool to automatically generate 3D meshes for EIT image reconstruction from a set of points, so the model was simplified using an extrusion technique. The `mk_extruded_model` function (Grychtol and Adler, 2013) in EIDORS v3.10 (Adler *et al.*, 2017a) was used to extrude the boundary of a single segmentation to a height of 20 cm. The 4^{th} intercostal space segmentation was used for extrusion. The lungs were specified 2 ways, the first method extruded 2D lungs, from the selected segmentation, and the second generated a 3D lung from all corrected slices of the lungs. To select a 3D lung, we selected all elements of the extruded mesh contained whin an alpha shape representation of the lung segmentation with an alpha value of 2 cm.

To generate a generic mesh for comparison the `mk_library_model` function in EIDORS was used which has available geometry for a cylindrical model with lung regions and a generic model of a human thorax. The conductivity of the lung regions was set to 0.7 of the background model conductivity.

All images were reconstructed using GREIT for 2D imaging (Adler *et al.*, 2009). For the GREIT reconstructions the noise figure was set to 0.5, 500 targets with a radius of 5 cm were used for training.

5.2.4 Evaluation on ARDS patients

Diagnostic CT data was acquired from 4 male patients aged 39–74. All patients were diagnosed with ARDS. EIT data were recorded using the Draeger EIT system on all patients with a 2D arrangement of 16 electrodes placed at the 4^{th} intercostal space.

All patients were mechanically ventilated at the time of recordings, but the exact ventilation parameters were unknown.

To evaluate the effect of the custom models on lung sensitivity, the centre of mass was computed for both the ventilation region detected in CT images, and the breath volume reconstructed in CT images. The centre of mass was calculated from EIT images by removing all positive changes in the image, then locating the centre of mass of all pixels that were over 50% of the ventilation signal amplitude. The breath used for calculated was an ensemble average representative breath of all breaths in the signal. The error in the centre of mass was calculated between the EIT reconstructed breath and the CT segmentation in the number of pixels.

5.3 Results

The goal of the automatic segmentation algorithm was to generate segmentations that were accurate for quick and easy manual correction. Figure 5.9 shows the result of the automatic segmentation regions. the red overlay indicates the healthy lung segmentation, and the orange overlay indicated regions that were added using the estimation method. The lungs were examined visually to determine how much manual correction was required. During testing we found that the level of accuracy was sufficient to complete segmentation correction for each subject in under 1 minute.

The segmentation results show that there is good identification of the ventilated lung region from the automatic segmentation. The estimated lung regions also helped to give starting approximations for the lungs and decrease required manual correction

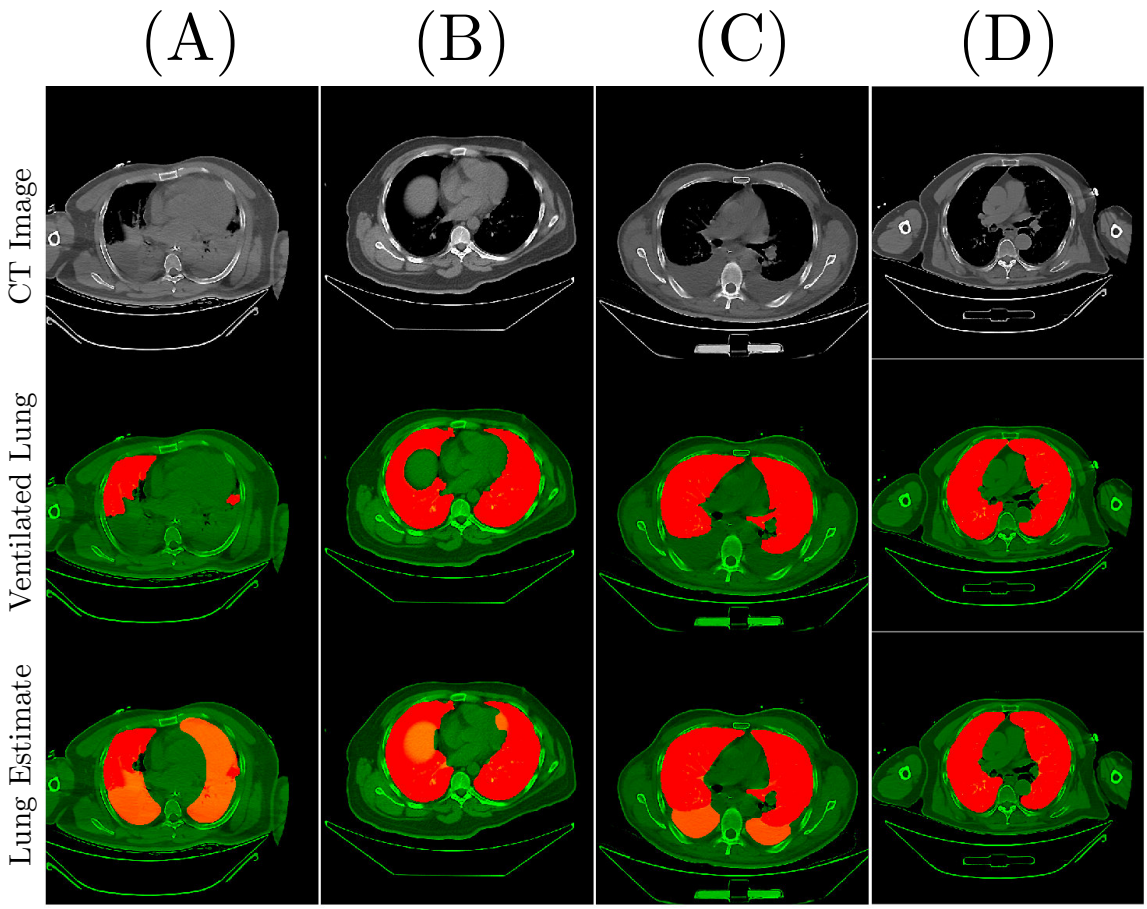

Figure 5.9: This figure shows the results of the automatic segmentation algorithm. The letters A–D represent the 4 patients. Patient A had a significant portion of the lung that was not ventilated, so an estimate was required to obtain lung regions. The ventilated lung estimate is shown in red on the 2nd and 3rd columns. The total lung area using the chest cavity and ventilated lung area is shown in the bottom row.

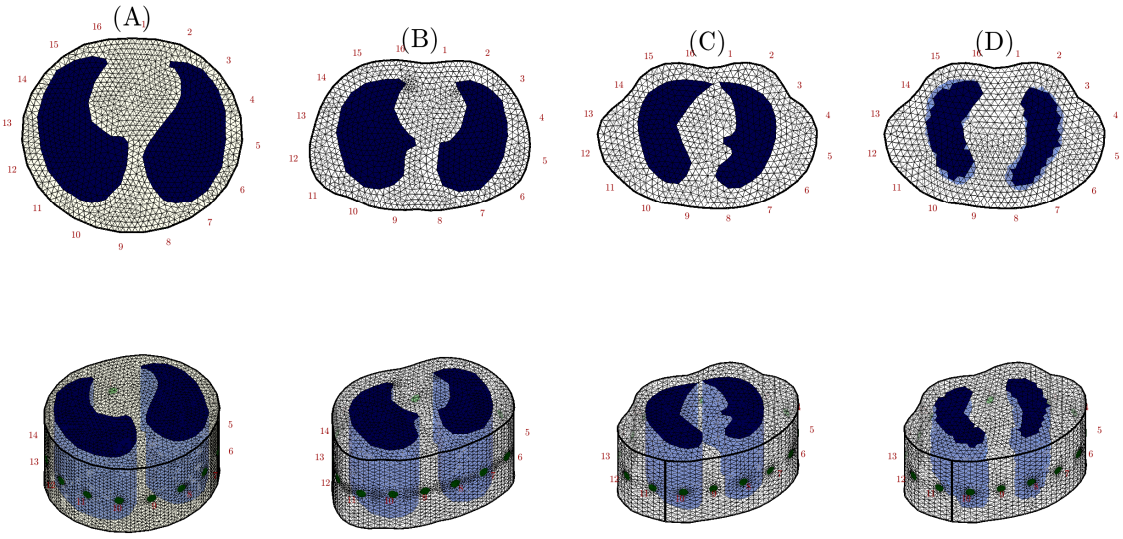

Figure 5.10: Example meshes and electrode locations for subject C (from figure 5.9). Model (A) is circular with lung regions. Model (B) uses the generic chest model from EIDORS and models (C) and (D) use the custom segmentation boundaries. Model (C) uses 2D lung boundaries from the 4th intercostal space extruded for the model height. Model (D) selects all elements are within the 3D lung boundary identified by the segmentation results.

time when there was limited ventilated lung in the available CT image. Sample meshes generated from the segmented images are shown in figure 5.10 for subject C (in figure 5.9).

For each patient there was a single EIT recording ranging from 30 – 60 seconds in length. To determine the improvement for the new customized meshes the ventilation pattern from the CT image was compared to the reconstructed ventilation on 4 types of models. The 4 types of meshes compared are pictured in figure 5.10: The first mesh was cylindrical with approximate lung regions, the second mesh was a generic model for an adult thorax, and the final two meshes were created from the segmentations. To compare the performance across all models, the centre of mass was compared

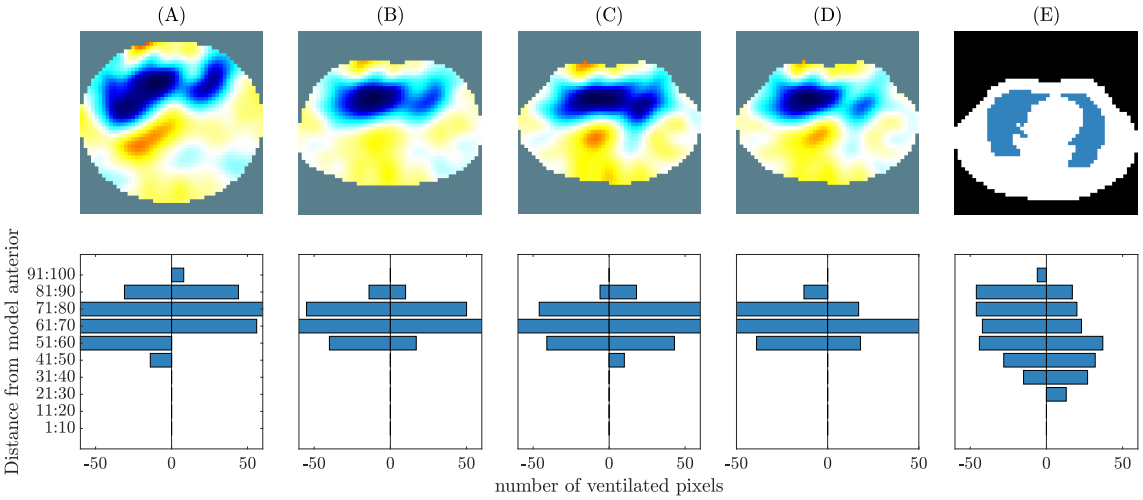

Figure 5.11: Example ventilation distribution for subject C (from figure 5.9). Column A and B are the generic models from the EIDORS library. Columns C and D show the custom models with 2D lungs (C) and 3D lung regions (D). Column E shows the distribution of the ventilated lung as segmented from the CT image.

between the CT imaged ventilation and the EIT imaged ventilation.

Reconstructed images in figure 5.11 show a very limited difference in ventilated regions and centre of mass between custom and generic models. There is a noticeable change in ventilation distribution using the circular model, but the generic thorax model and the custom models show very similar results. There is a slight shape difference in the ventilation distribution between the generic thorax model and custom models, but there is very little measurable difference.

Error in the centre of mass across all models for all subjects was calculated and is shown in figure 5.12. The error is estimated as the distance in pixels between the venter of mass of the ventilated lung from the CT estimate and the centre of mass of the reconstructed breath.

The centre of mass error was not significantly different across all models for each

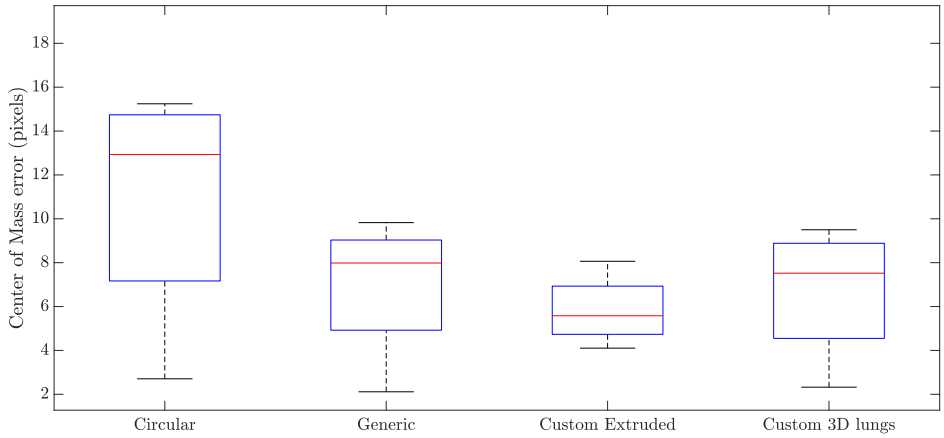

Figure 5.12: Example ventilation distribution for subject C (from figure 5.9). Column A and B are the generic models from the EIDORS library. Columns C and D show the custom models with 2D lungs (C) and 3D lung regions (D). Column E shows the distribution of the ventilated lung as segmented from the CT image.

of the subjects. The average error for the circular model was slightly higher than the customized geometry, but for all models the centre of mass, and shape of the ventilation distribution was similar. It is not clear that custom models improved reconstruction accuracy of breath reconstructions in the EIT images. There are several factors that may contribute to this.

5.4 Discussion

The goal of this chapter was to create a tool to automatically segment CT images from ARDS patients to improve lung sensitivity to improve individualized ventilation monitoring. An automatic segmentation algorithm was developed to give a baseline segmentation of the lungs which gave an accurate starting point of the true lung

boundary. A tool for manual correction was designed that enabled quick, accurate corrections of automatically generated CT images. Segmented images were used to generate meshes with accurate boundary shapes and lung outlines.

Although it has been shown that accurate models of the boundary and lung improve measures of GI index (Yang *et al.*, 2021), the models with improved boundary accuracy in this chapter did not show this improvement. One factor that was different between the two studies was the value of lung conductivity. Yang *et al.* (2021) used a conductivity value of 1.3 for the lung tissue relative to the model background. This is atypical since the conductivity of lung tissue is considerably lower than other tissues in the body. In this chapter using a value of 1.3 times the background conductivity did not improve the centre of mass error across custom models.

There are several other factors that may contribute to the mismatch between the CT ventilation and the EIT imaged ventilation. First, the difference in posture and condition between the CT and the EIT image was not known. The EIT belt was not in position during the CT scan, so there was potential that the patient position and posture were slightly changed. Although this may contribute to a slightly different shape of the thorax, it is not likely to drastically change the boundary of the chest cavity. One of the larger factors is likely the unknown locations of the electrodes. Since the exact location of the electrode is unknown, the 16 electrodes were placed evenly around the thorax. Incorrect electrode locations can have a large impact on the resulting EIT image, resulting in artefact and lower reconstruction accuracy (Boyle and Adler, 2011). Since the CT images acquired contain spatial information, there is potential to improve accuracy of the electrode placement on the models.

The EIT system used has several available belts with different electrode spacing and points of attachment. If the user was able to select the belt used and the attachment point or tightness in the software, the electrode locations could be more easily approximated. Alternatively, an image or CT with the electrode belt in place could allow precise estimation of the electrode location and spacing. It may also be feasible to reconstruct the electrode location partially using a movement jacobian (Soleimani *et al.*, 2006), although it is not currently possible to do this with the GREIT algorithm.

On top of improving the accuracy of the electrode placement in the meshes there is still future development planned for the segment editor and automatic segmentation. Initial tests were done on the CT and EIT data from 4 patients, and validation across a wider dataset is required to ensure stability of the automatic segmentation and ease of editing. Improvements to the appearance of the interface and documentation must also be added before the software is easy to use in a clinical setting. Work is currently underway to obtain several more sets of CT and EIT data to validate the automatic segmentation and manual correction steps.

It was noted in the reconstructions that when using the 3D lung region model there was a slight reduction in the amplitude of a conductive artefact that appeared in the center of the iamges. It is possible that the the 3D aspect of the model allows the 3D path of the current to be modelled more accurately (Adler and Boyle, 2017), but the extent of the benefit is limited when using a 2D arrangement of electrodes (Grychtol *et al.*, 2016).

When creating meshes using the `ng_mk_extruded_model` in EIDORS (Grychtol

and Adler, 2013), accurate models with a good representation of the boundary are created, but Netgen occasionally fails to mesh the electrodes on models. We presume this is due to irregular and concave curves. This occurred several times on the segmented data, and a more robust meshing or electrode placement technique will be required. Placing 3D lung boundaries helped to reduce errors that were introduced by tight corners on lung segmentations, but electrode and boundary meshing errors were still present in this model.

5.5 Summary

The diagnostic CT images required for ARDS diagnosis are an excellent source of spatial information about the size and locaiton of organs in a subject. An segmentation and boundary editing tool was developped to generate accurate meshes of the external and lung boundaries from CT images. In ARDS patients with very poor lung health segmentation of the actual lung boundary is challenging, but with a multi-step process including chest cavity segmentation and manual verification, we generated accurate, custom meshes for a small number of ARDS patients. The benefits of custom meshes were not clear on this small sample size, although additional steps to improve electrode localization may improve results. Work is currently underway to validate and improve the segmentation tool on a larger dataset of ARDS patients. Methods to reduce the impact of sentisitivity to electrode location error on reconstructions, or correctly identify correct electrode locaitons could help make this technique more viable.